RSC Advances

PAPER

View Article Online
View Journal | View Issue

Cite this: *RSC Adv.*, 2017, **7**, 5067

Fabrication of two-layer dissolving polyvinylpyrrolidone microneedles with different molecular weights for *in vivo* insulin transdermal delivery

I.-Chi Lee,†[ab] Yu-Chieh Wu,†[a] Shau-Wei Tsai,[a] Chih-Hao Chen[c] and Min-Hsien Wu*[ade]

Transdermal drug delivery is a convenient route to transport pharmaceuticals. However, its application is limited to a few compounds. Microneedle (MN) patches have demonstrated a high efficiency for delivering poorly permeable drugs and gained significant attention due to the advantages of being painless and convenient for patients as well as providing efficient delivery. This study presents dissolvable polyvinylpyrrolidone (PVP)-based MNs that do not require needle removal while providing the rapid release of encapsulated insulin. PVP with two molecular weights, PVP10 and PVP360, were used to fabricate the needle portion of the MNs, and PVP360/sodium carboxymethyl cellulose (CMC) was used for preparation of the backing layer. The detailed characteristics and *in vitro* skin penetration capability of a series of PVP360/PVP10 MNs were analyzed. The penetration depths of PVP MNs were evaluated using optical coherence tomography. The PVP360/PVP10 = 1 : 3 MN patch was chosen for *ex vivo* and *in vivo* studies. *Ex vivo* drug release profiles show that the permeation efficiency of Lissamine green B (LGB)- and fluorescein isothiocyanate-labeled BSA (FITC-BSA)-loaded PVP MN patches was much higher than the groups of patches without MNs. Furthermore, to estimate the feasibility of PVP MNs for diabetes treatment, insulin-loaded PVP MN patches were administered to diabetic mice to evaluate glycemic control. The relative pharmacologic availability revealed that the MN patch has an immediate and effective effect on hypoglycemic administration. This study demonstrates that dissolvable PVP MNs may serve as a promising device to deliver macromolecules or protein drugs for efficient transdermal drug delivery.

Received 29th November 2016
Accepted 20th December 2016

DOI: 10.1039/c6ra27476e

www.rsc.org/advances

1 Introduction

Transdermal drug delivery (TDD) systems provide good patient compliance and are used for controlled and pain-free drug delivery. The TDD system utilizes the skin as a portal to deliver biotherapeutics into the systemic circulation while avoiding possible degradation due to the gastrointestinal tract or first-pass liver effects.[1] However, hypodermic needles have been a gold standard for pharmaceutical or protein delivery for over a century because TDDs are only useful for transporting small or oil-soluble molecules due to the difficulty of penetrating the stratum corneum barrier. In the past, successful drug delivery across intact skin has been related to the physicochemical properties of the drug, such as molecular weight (<500 Da), potency of the drug and partition coefficient. Dissolvable microneedles (MNs) offer an attractive solution for pharmaceutical transportation and have received significant attention for their painless and efficient delivery, biocompatibility, low cost, convenient fabrication, and high drug loading. Compared with metal or silicon MNs, there are no safety concerns if MNs break off in the skin, and there is no sharp biohazardous waste.[2,3]

Poor glucose control and insulin deficiency are the hallmarks of diabetes. Optimal glycemic control is essential for minimizing the risk of diabetes-induced complications. Hypodermic injection is the most effective glucose management for patients with insulinopenia. However, many patients are concerned about self-injection. Consequently, nasal, gastrointestinal, and inhalation therapy for insulin transportation have been developed to replace hypodermic injection. However, thus far, there are considerable

[a]*Graduate Institute of Biochemical and Biomedical Engineering, Chang-Gung University, No. 259, Wenhua 1st Rd., Guishan Dist., Tao-yuan 33302, Taiwan, Republic of China. E-mail: mhwu@mail.cgu.edu.tw; Tel: +886 3 2118800 ext. 3599*

[b]*Neurosurgery Department, Chang Gung Memorial Hospital, Tao-yuan 33305, Taiwan, Republic of China*

[c]*Department of Plastic and Reconstructive Surgery, Chang Gung Memorial Hospital, Tao-yuan 333, Taiwan, Republic of China*

[d]*Division of Hematology/Oncology, Department of Internal Medicine, Chang Gung Memorial Hospital at Linkou, Tao-yuan City 333, Taiwan, Republic of China*

[e]*Department of Chemical Engineering, Ming Chi University of Technology, New Taipei City, Taiwan, Republic of China*

† I.-Chi Lee and Yu-Chieh Wu contributed equally to this work.

drawbacks regarding efficiency, side effects, or patient acceptance.[4–6] Dissolvable MN patches loaded with insulin are an alternative solution for an effective, painless, discreet, and self-administered method for glucose regulation.[7,8]

Several types of dissolving polymers have been used in previous studies to fabricate soluble MNs, including collagen, hyaluronic acid,[9,10] PMVE/MA,[11,12] carboxymethylcellulose (CMC),[8,13] polyvinylpyrrolidone (PVP),[14,15] sodium alginate,[16] and silk.[17] Mechanical properties, material cost, fabrication convenience, and inflammation risk are the important parameters when choosing materials. Among these popular materials, PVP is widely used and has been approved by the U.S. Food and Drug Administration (FDA) for several purposes, such as a coating agent, polymeric membrane, and material for controlled drug release.[18] Furthermore, PVP has also been used for a long time as a blood plasma expander in a clinical setting.[19] In addition, PVP with a molecular weight of less than 20 kDa is efficiently removed from kidneys after injection and is thus safer to use.[15]

PVP MNs may achieve rapid dissolution when inserted into skin and could be fabricated at a mild temperature without the need to use organic solvents. Although PVP has been reported to make MNs, the poor mechanical properties restrict its broad applications, especially low molecular PVP.[15]

The purpose of this study was to develop rapid dissolvable insulin-loaded MN patches fabricated from polyvinylpyrrolidone (PVP) with different molecular weights and to estimate the applicability for insulin transdermal delivery in diabetic mice. PVP with two molecular weights, PVP10 and PVP360, was used to fabricate the needle portion, and the best ratio of PVP10/PVP360 was chosen for optimizing mechanical properties. Additionally, appropriate backing material was also assessed. *In vitro* skin penetration capability and penetration depth of several ratios of PVP10/PVP360 MNs were analyzed. *Ex vivo* delivery profiles of Lissamine green B (LGB) and bovine serum albumin (BSA) were determined using the Franz diffusion cell system, and the vertical delivery of BSA was investigated using confocal microscopy. Finally, because of its clinical relevance, insulin was selected as a model drug to validate the feasibility of using PVP MNs encapsulated with insulin to regulate glucose levels in an animal model.

2 Materials and methods

2.1 Materials for the preparation of two-layer dissolving PVP-based MN patches

The commercial microchannel Skin System MN patches purchased from 3M™ were used as the master mold. Polydimethylsiloxane (PDMS) (Sylgard 184, Dow Corning, Belgium) was used to manufacture the female mold. PVP10 (molecular weight (MW): 10 kDa), PVP360 (MW: 360 kDa), carboxymethylcellulose sodium salt (MW: 90 kDa) (CMC), Lissamine green B (LGB) (MW: 576.62 Da), bovine serum albumin (BSA) (MW: 66 kDa), fluorescein 5(6)-isothiocyanate (FITC) (MW: 389.38 Da), and human insulin (potency ≥ 27.5 units per mg, MW 5.807 kDa) were purchased from Sigma-Aldrich, USA.

2.2 Fabrication of two-layer dissolving PVP-based MN patches

In this study, 3M™ MN patches were used as master templates to fabricate MN female molds with PDMS, as previously described.[20] The two-step fabrication process was based on the previous studies with modifications. In total, 4 different weight ratios of 30% polymer solutions, PVP360/PVP10 (1 : 1, 1 : 2, 1 : 3, 1 : 5), loaded with model drugs were prepared, poured into PDMS molds, and centrifuged in swinging bucket rotors (KUBOTA 2420, Japan) at 3500 rpm for 30 minutes to fill the MN patch mold cavities. The residual solutions on the mold surfaces were removed and dried for 10 minutes at room temperature (R.T.), followed by another centrifugation at 3500 rpm for 30 minutes and dried at R.T. overnight. Subsequently, a second layer of high molecular weight PVP solution, 30% PVP360, without drug mixing, was poured into the PDMS molds as the second layer and centrifuged at 3500 rpm for 10 minutes. Then, the MN patch molds were dried at R.T. overnight and preserved in dry conditions.

2.3 Manufacturing of drug-loaded MN patches

LGB, a water-soluble blue-green dye with an absorption wavelength of 633 nm, was mixed into the PVP solutions and used as a low molecular weight model drug. BSA-FITC, as a high molecular weight model drug with an excitation wavelength of 495/525 nm, was dissolved in the PVP solutions as well. In the animal model test, the model drug, insulin, was dissolved in a 0.1 M HCl solution and then added to the PVP solutions to form the first layer of MNs. In addition, a 30% PVP360 solution containing 25% CMC was loaded as a backing layer, as shown in Fig. 1 – process B, to improve the flexibility of MN molds. The morphologies of drug-loaded MN patches were investigated using stereomicroscopy (OLYMPUS, SZ2-ILST) and an inverted fluorescence microscope (NIKON, ECLIPSE Ti-S). Additionally, the drugs located in the needle tip of the MN patches were observed.

2.4 Morphology of MNs and characteristics analysis

Detailed characteristics of PVP MN patches were observed using scanning electron microscopy (Hitachi, S-3000N). The height, width and interspace of the PVP360/PVP10 MN patches were measured using ImageJ software.

2.5 *In vitro* skin penetration

To evaluate the *in vitro* skin insertion capability of the two-layer dissolving PVP MNs, the LGB-loaded MNs were inserted into porcine cadaver skin *via* a handmade applicator with a force of 12 N per patch for 10 seconds and then peeled off.

2.6 Optical coherence tomography

To analyze the insertion ability and the penetration depth, different ratios of PVP360/PVP10 MNs were implemented with an application force of 12 N per patch for 40 seconds without peeling them off. PVP MNs were inserted into porcine cadaver skin and were observed using optical coherence tomography (OCT) (Chang Gung University, Taiwan) with an MEMS-based swept source. To observe the morphology of created holes and

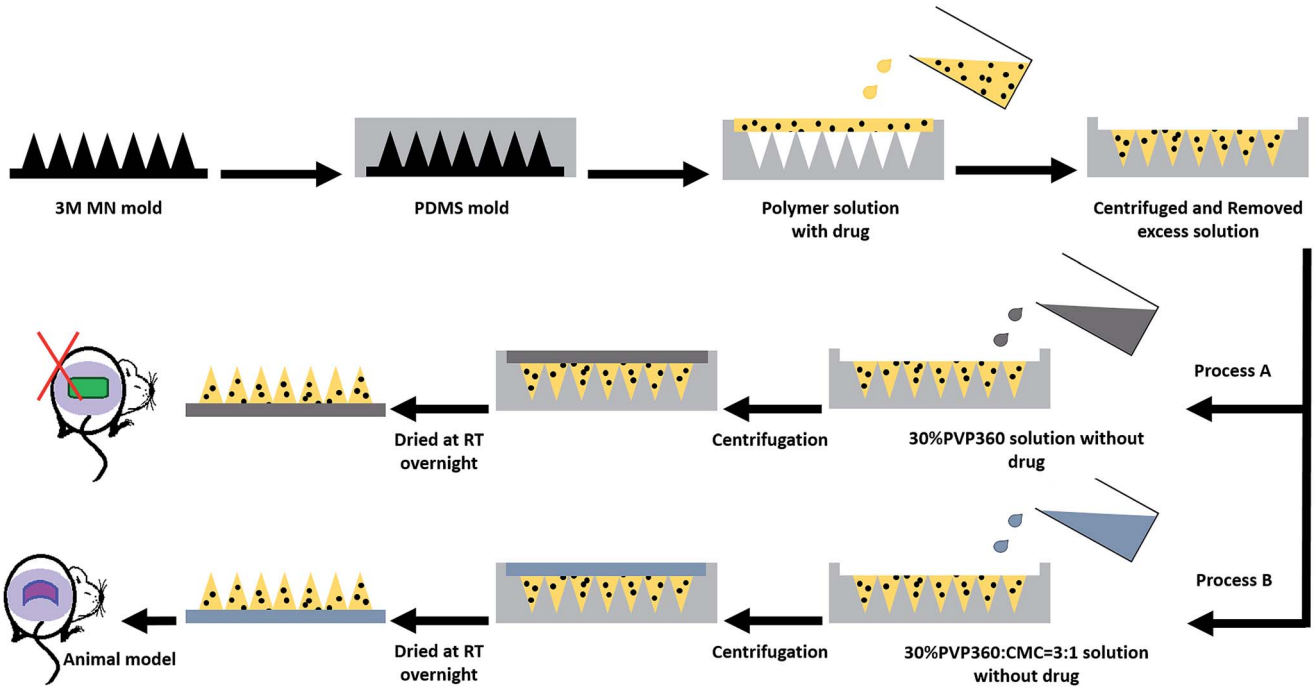

Fig. 1 Schematic illustration of the fabrication process of the two-layer PVP360/PVP10 MN patches. Process A illustrates the PVP360/PVP10 MN patches-encapsulated model drugs with a backing layer that is made from the PVP360 polymer solution. Process B illustrates the PVP360/PVP10 MN patches-encapsulated insulin with a backing layer composed of the PVP360/CMC polymer solution for animal studies.

the repair ability of porcine cadaver skin after penetration, porcine skin was observed immediately after peeling off the MN patches. The operation parameters were followed as described in our previous study.[8] Skin penetration depths for different ratios of PVP MNs and the degree of skin repair were observed immediately without histological sections.

2.7 *In vitro* transdermal delivery of BSA-FITC-loaded PVP360/PVP10 MN patches

To visualize the TDD of the MN patches, the BSA-FITC-loaded PVP360/PVP10 = 1 : 3 MN patches were inserted into porcine cadaver skin with an application force of 12 N per patch and then were removed after 10 minutes. The varying depths from the skin surface in the vertical direction were recorded using a confocal laser scanning microscopy (Zeiss, 510N).

2.8 *Ex vivo* model drug delivery tests

An *ex vivo* study of model drug delivery on porcine cadaver skin was performed using Franz diffusion cells (Intek glass, 5 ml, Taiwan). PVP360/PVP10 MN patches loaded with LGB or BSA-FITC were placed on the porcine skin, and the patch without MNs was used as the control group. The preparation method of patches without MN was followed by (a) grinding off the needles of the 3M mold and (b) fabricating the patches *via* the same method described previously. Porcine skins were mounted onto Franz cells and were secured to the donor compartment of the diffusion cell using medical adhesive tape (AsDerma Suprasorb F Film Medical Adhesive Tape) with the SC side facing the donor compartment. The receptor medium (5.5 ml of 1× PBS, pH 7.4) was maintained at 32 °C and stirred (600 rpm) continuously. The concentrations of LGB and BSA-FITC in the receiver media were measured using an Enzyme-Linked ImmunoSorbent Assay (ELISA) reader, and the percentages of cumulative permeation over time were measured.

2.9 *In vivo* delivery efficacy tests

To evaluate the drug delivery efficacy of PVP MN patches, 0.2 IU insulin-loaded PVP MN patches were prepared, analyzed and corrected using an ELISA kit (ALPCO, NH, USA). The diabetic mice were induced as described in a previous study.[8] All animal experiments were approved by the Chang Gung University in accordance with the guidelines for animal experimentation (IACUC approval number: CGU15-044). Male BALB/c mice with an average weight of approximately 27 g (provided by the National Laboratory Animal Center, Taiwan) were injected with streptozocin (STZ, Sigma, USA) in 0.1 ml of a sodium citrate buffer (0.05 M, pH 4.5), 200 mg kg^{-1}. After 1 week, the blood glucose levels of mice were confirmed using a glucometer (ACCU-CheckVR Active, Roche, Germany).

All diabetic mice with a glucose level exceeding 300 mg dl^{-1} were divided into four groups ($n \geq 5$): (a) the insulin-loaded PVP MN patch group (0.2 IU insulin-loaded MN patches), (b) the subcutaneous group (0.2 IU insulin solution), (c) the unloaded PVP MN patch group, and (d) the control group, diabetic mice without any treatment. MN patches and hypodermic injections were given to the diabetic mice. There was no feeding after administration. At 0, 1, 2, 3, and 4 hours after administration, the plasma glucose levels *versus* time were measured using the glucometer.

2.10 *In vivo* pharmacodynamics analysis

The profile of plasma glucose *versus* time was plotted, and the minimum glucose level (C_{min}) and the time point of minimum glucose level (T_{min}) were measured from the curves. The area above the curves (AAC) for 0–4 hours was estimated using the trapezoidal area formula. The relative pharmacological availability (RPA) was calculated using the following equation:

$$\text{RPA}\ (\%) = \{(\text{AAC}_{\text{MN}}) \times (\text{dose}_{\text{SC}})\}/\{(\text{AAC}_{\text{SC}}) \times (\text{dose}_{\text{MN}})\} \times 100$$

where AAC_{MN} indicates the area of AAC after applying the insulin PVP-based MN patches, and AAC_{SC} reveals the area above the curve after applying the subcutaneous injection (SC) of insulin.

2.11 Statistical analysis

The data are presented as the mean ± standard deviation (SD) of four to six independent experiments. The results were analyzed *via* Student's *t* test. Statistical significance is indicated as ** for $p < 0.01$ and *** for $p < 0.005$.

3 Results and discussion

3.1 Fabrication of dissolving PVP360/PVP10 MN patches

In our previous study, a 3M mold was used as the master mold to prepare PVP/PVA polymeric MN patches and successfully regulate the drug release rate.[4] Herein, the 3M mold with pyramidal MNs was chosen as the master mold because previous literature has revealed that pyramidal MNs show better mechanical strength than conical type MNs due to the small aspect ratio, which is especially suitable for mechanically weak biomaterials.[13] Dissolvable MN patches have been proven to increase skin permeability and enhance drug delivery efficiency.[13,21,22] The two-step casting process is easy for localizing the drugs in the needle tip for more effective drug utilization.[21–23] Fig. 1 is the schematic illustration of the fabricating process of the dissolving PVP360/PVP10 MN patches. In the first step, different ratios of PVP360/PVP10 polymer solutions (1 : 1, 1 : 2, 1 : 3, 1 : 5) were mixed with the drug, then this solution was added into the PDMS mold cavities, and the drug was localized in the tips *via* centrifugation for 30 min. Then, the polymer solution without drug mixing was loaded into the first

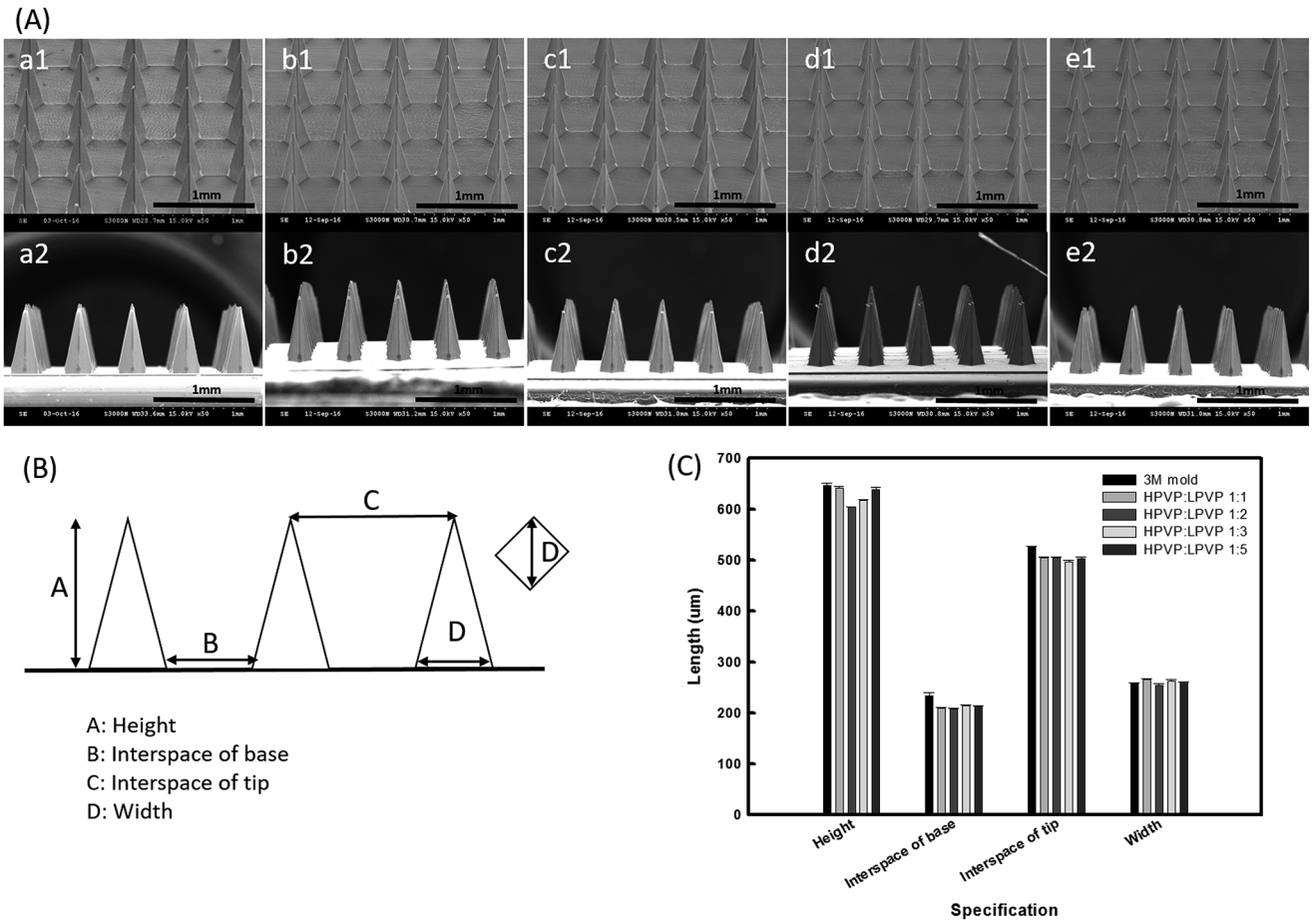

Fig. 2 Detailed dimensions of a series of PVP360/PVP10 MN patches. (A) Scanning electron microscopy images of PVP360/PVP10 MN patches: (a1–a2) 3M mold, (b1–b2) PVP360 : PVP10 = 1 : 1, (c1–c2) PVP360 : PVP10 = 1 : 2, (d1–d2) PVP360 : PVP10 = 1 : 3, (e1–e2) PVP360 : PVP10 = 1 : 5. (B) Diagrammatic representation of the MN array and its geometric parameters. (C) Detailed dimensions of the 3M mold and the four weight ratios of the two-layer PVP MN patches.

layer and centrifuged for 10 min to form a backing layer. The PVP-based MN patches prepared by processes A and B were used for *in vitro* and *in vivo* tests, respectively.

3.2 Characteristics of PVP360/PVP10 MNs

Fig. 2(A) demonstrates the morphologies of 3M molds and the four ratios of dissolving PVP360/PVP10 MN patches, which indicate that these MN patches were successfully replicated from the 3M molds. Fig. 2(B) is the diagrammatic representation of the MN array and related geometrical parameters. The detailed dimensions of each MN patch were measured using the ImageJ software and are shown in Fig. 2(C). As shown in Fig. 2(C), it is demonstrated that the losses of the characteristics, including the height, width, interspacing tip, and interspacing base of the four ratios of PVP MNs, were all <10% compared with the original 3M mold.

3.3 Insertion capability of PVP360/PVP10 MN patches

To compare the skin insertion capability of four different ratios of PVP360/PVP10 MN patches, LGB-loaded PVP MN patches were punctured into porcine cadaver skin with an application force of 12 N per patch. Fig. 3(A1)–(D1) demonstrates that LGB dyes were successful encapsulated and localized in the tip of a series of PVP360/PVP10 MN patches. After a 10 second insertion, PVP MN patches were removed and imaged using stereomicroscopy, as shown in Fig. 3(A2)–(D2). It was demonstrated that the four types of PVP360/PVP10 MN patches dissolve in porcine cadaver skin immediately after the insertion. Fig. 3(A3)–(D3) shows the result of porcine cadaver skin after the penetration and patch removal, and the blue-green spots revealed a high insertion ratio from each PVP360/PVP10 MN (approximately 100%). The insertion holes were observed more clearly in magnified images, as shown in Fig. 3(A4)–(D4).

3.4 Real-time investigation of MN insertion *via* OCT

In our previous studies, we used OCT to visualize the image in real time while MNs were successfully inserted into the skin.[20] Herein, OCT also provides a function of measuring the exact depth of the MN patch penetration. Fig. 3 shows the confirmation of puncture ability of different ratios of PVP360/PVP10 MNs. However, the technique cannot provide either the information inside the skin surface or the exact depth of penetration. Therefore, Fig. 4 demonstrates real-time images of the *in vitro* PVP360/PVP10 MNs insertion using OCT. Fig. 4(A) shows the porcine skin before penetration, and Fig. 4(B) and (C) show the porcine skin punctured by PVP MN patches and after MN patch removal, respectively. The location of microdisruptions in the skin was clearly observed. This suggests that the four ratios of PVP360/PVP10 MN patches all demonstrated the capability to

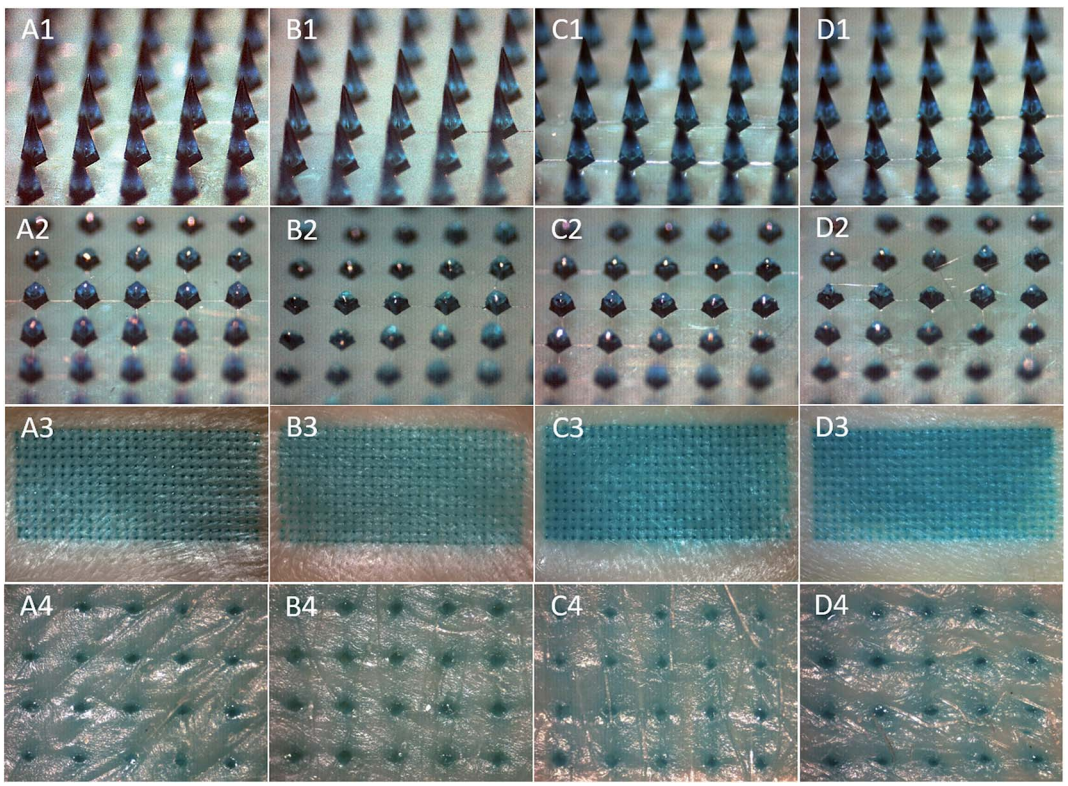

Fig. 3 *In vitro* skin insertion capability of LGB-loaded PVP360/PVP10 MN patches; (A1–A4) 30% PVP360/PVP10 = 1 : 1, (B1–B4) 30% PVP360/PVP10 = 1 : 2, (C1–C4) 30% PVP360/PVP10 = 1 : 3, and (D1–D4) 30% PVP360/PVP10 = 1 : 5. (A1–D1) Stereomicroscopy images of the MN patches before insertion. (A2–D2) Stereomicroscopy images of the MN patches after 10 seconds of insertion. (A3–D3) Porcine cadaver skin after the insertion of the LGB-loaded PVP360/PVP10 MN patches after 10 seconds and after patch removal. (A4–D4) Magnified images of porcine cadaver skin after MN insertion and patch removal.

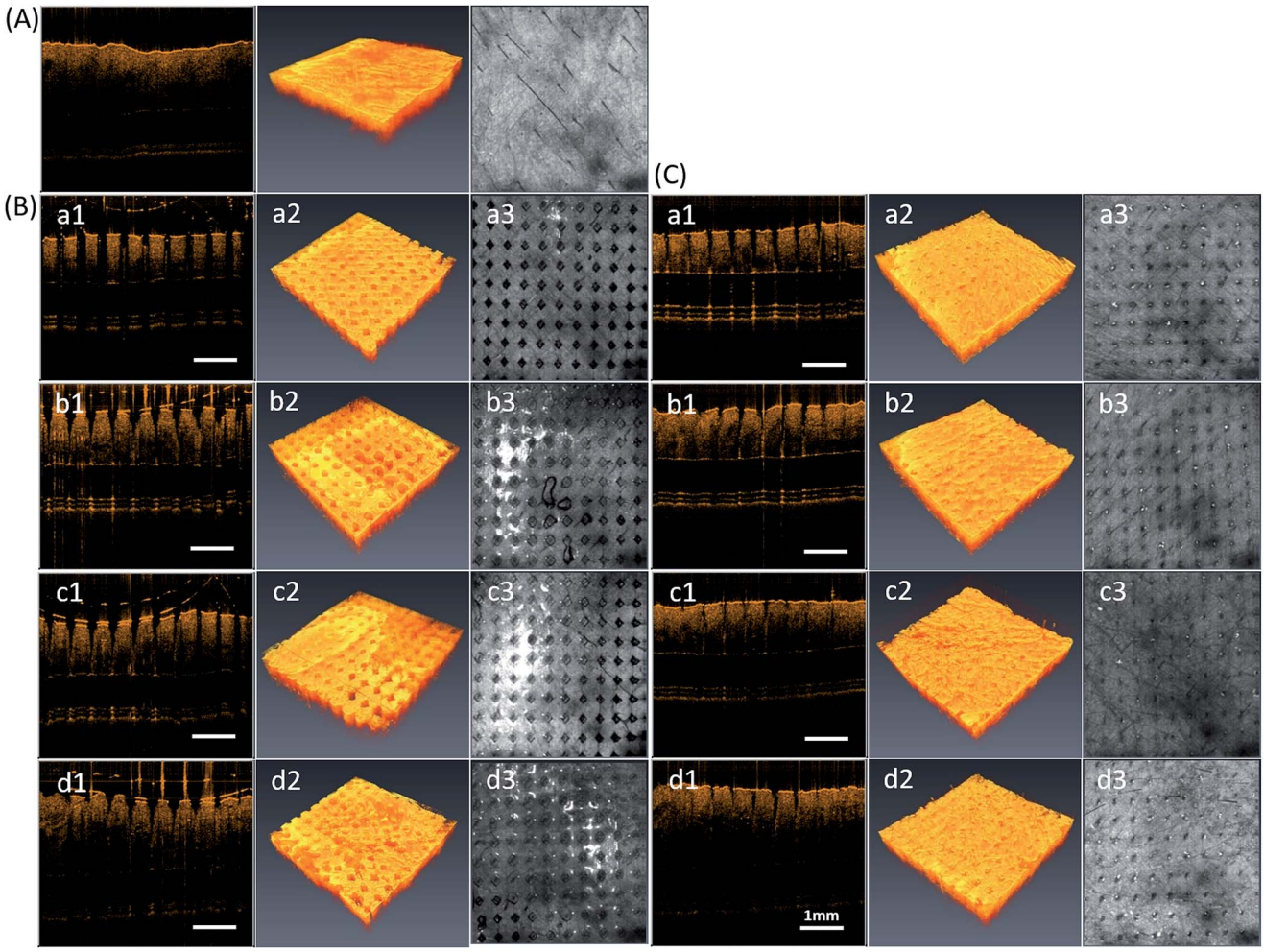

Fig. 4 OCT images of PVP360/PVP10 MN patches penetrating porcine skin. (A) Porcine skin before puncturing. (B) Porcine skin after puncturing with MN patches that include PVP360/PVP10 1 : 1 (a), 1 : 2 (b), 1 : 3 (c), 1 : 5 (d), respectively. (C) Porcine skin after the MN patches are removed. (B, C, row 1) 2D images of the cross-section. White arrows highlight the location of microdisruptions in the skin; (B, C, row 2) 3D reconstruction images; (B, C, row 3) en face images at a depth of 300 μm beneath the tissue surface.

puncture the stratum corneum (SC) barrier. Fig. 4(B, a1–d1) shows the cross-sectional images, and the depth of penetration that is beneath the tissue surface was greater than 300 μm. Three-dimensional reconstruction images are shown in Fig. 4(a2–d2), and the top-view images are shown in Fig. 4(a3–d3). The pattern of holes formed by the PVP360/PVP10 MN patches was observed, and the microholes with a diameter of approximately 200 μm were also investigated. The pattern size is consistent with the mold. The effect of penetration, as shown in Fig. 4(B, a and b), shows that larger and deeper microholes may due to the higher ratio of PVP360 in PVP360/PVP10 MN patches. It is demonstrated that the better mechanical properties of PVP360 may result in better puncture ability. Despite their stronger mechanical penetration abilities, the skin was unable to heal immediately after the patches were peeled off, as shown in Fig. 4(C, a and b). In contrast, Fig. 4(B, d) shows the least depth of penetration (less than 300 μm). Consequently, OCT analysis shows that the exact depth of penetration is related to the weight ratio of the PVP360/PVP10 polymer solution. A previous study has also revealed that the chemical backbone structure of the vinyl pyrrolidone monomer contains a ring that may increase intramolecular rigidity, and therefore, PVP360 may provide a better mechanical strength than PVP10.[15] This means that the OCT analysis is consistent with previous literature. These results indicate that the PVP360/PVP10 1 : 3 MN patches present a sufficient capability of penetration *via* SC to create microholes, and the healing rate of the skin is faster than the PVP360/PVP10 ratio of 1 : 1 and 1 : 2 MNs after the MN patch is peeled off. In addition, the previous study revealed that PVPs with a low molecular weight are efficiently removed from kidneys and are safer to use.[15] Consequently, the PVP360/PVP10 ratio of 1 : 3 MNs were chosen to evaluate the transdermal delivery efficiency in the following experiment.

3.5 *In vitro* transdermal delivery of BSA-FITC-loaded PVP360/PVP10 MN patches

To evaluate the feasibility of *in vitro* TDD efficiency, the BSA-FITC-loaded PVP360/PVP10 MN patch was inserted into

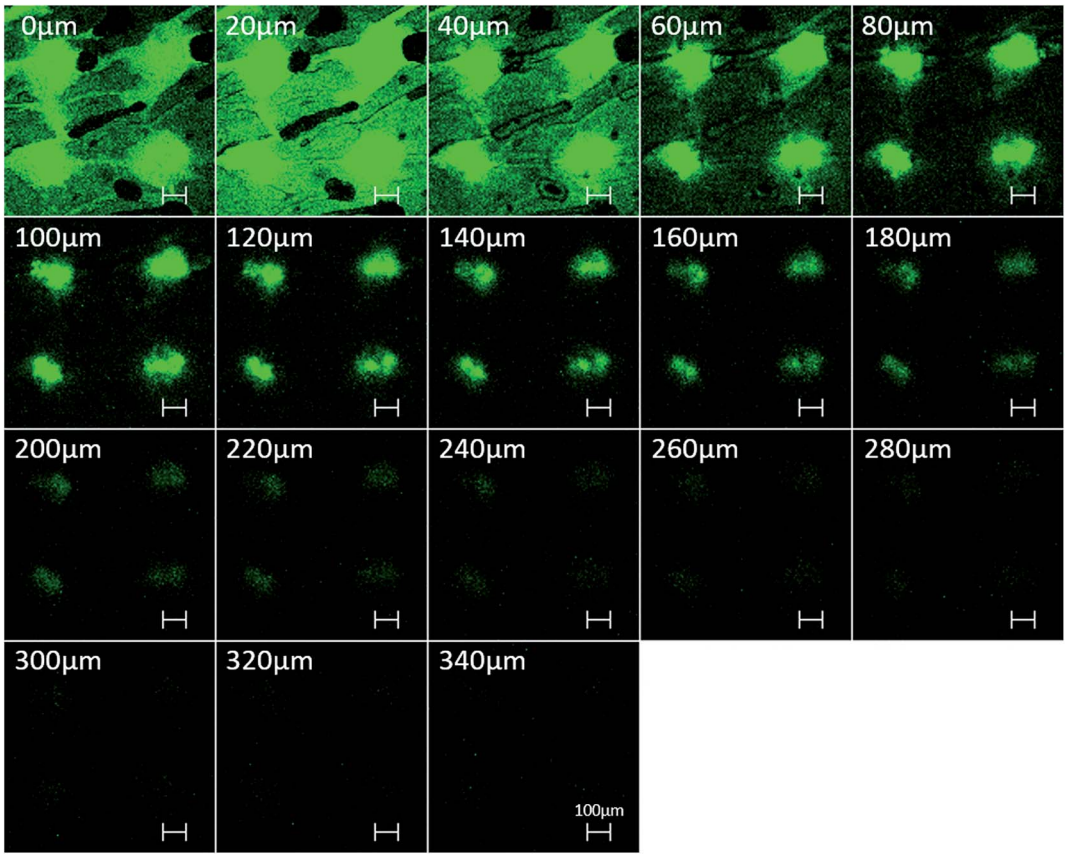

Fig. 5 *In vitro* transdermal delivery of BSA-FITC PVP360/PVP10 MN patches across porcine cadaver skin at varying depths after insertion for 10 min with a skin thickness of 340 μm. The amount of BSA-FITC that is loaded in the PVP360/PVP10 MNs is approximately 30 μg per patch.

porcine cadaver skin with an application force of 12 N per patch, removed after 10 min, and observed *via* confocal microscopy. The skin puncture site was imaged, scanned, and recorded at varying depths from the skin surface, as shown in Fig. 5. It was observed that the maximum depth of BSA-FITC drug diffusion was approximately 340 μm after only 10 minutes of insertion. Compared with previous studies,[20] because BSA is a large protein with a molecular weight of 66 kDa, the BSA loaded PVP360/PVP10 1 : 3 MN patches demonstrate a faster rate of transdermal delivery and a deeper drug diffusion depth in only 10 min than the PVP/PVA MNs. It is considered that the higher solubility of PVP360/PVP10 than of PVP/PVA MNs thereby results in a higher dissolution rate and affects the efficiency of transdermal delivery. This result indicates that the PVP360/PVP10 = 1 : 3 MNs show the potential to assist pharmaceutical transportation and enhance drug diffusion efficiency across the SC barrier layer.

3.6 *In vitro* drug delivery profile of LGB- and BSA-FITC-loaded PVP360/PVP10 MN patches

To evaluate the *in vitro* release profiles of the encapsulated drugs, LGB- and BSA-FITC-loaded PVP360/PVP10 MN patches with and without the needles were inserted into porcine cadaver skin, and the drug release was subsequently monitored for 120 hours. As shown in Fig. 6(A) and (B), both profiles show that the permeation efficiency of patches with MN groups was significantly higher than for the groups of patches without MNs. Fig. 6(A) demonstrates that the percentage of cumulative permeation was greater than 30% in only 6 hours, and it reached 80% after 60 hours. Because the molecular weight of BSA-FITC is higher than that of LGB, the delivery rates were significantly slower than those of LGB. However, even though a lower cumulative permeation in BSA-loaded MN patches was observed after 120 hours, the amount of cumulative permeation shows significant differences compared with the patches without MNs, as shown in Fig. 6(B). BSA is a very large protein with a molecular weight greater than 60 kDa. It is suggested that if PVP MNs encapsulate other pharmaceuticals that have a smaller molecular weight than BSA, a better cumulative permeation may be demonstrated.

3.7 Animal study of insulin-FITC-loaded PVP360/PVP10 MN on diabetic mice and pharmacodynamic analysis

The efficiency of insulin delivery *via* PVP360/PVP10 MNs was determined using diabetic mice, and the results after the application are shown in Fig. 7. The experimental groups included an insulin-loaded PVP360/PVP10 MN patch group, SC injection with insulin group, unloaded PVP360/PVP10 MN patch group, and the control group. During the animal studies, it was found that the backing layer of the original PVP MN patches prepared by process A in Fig. 1 is too rigid and is

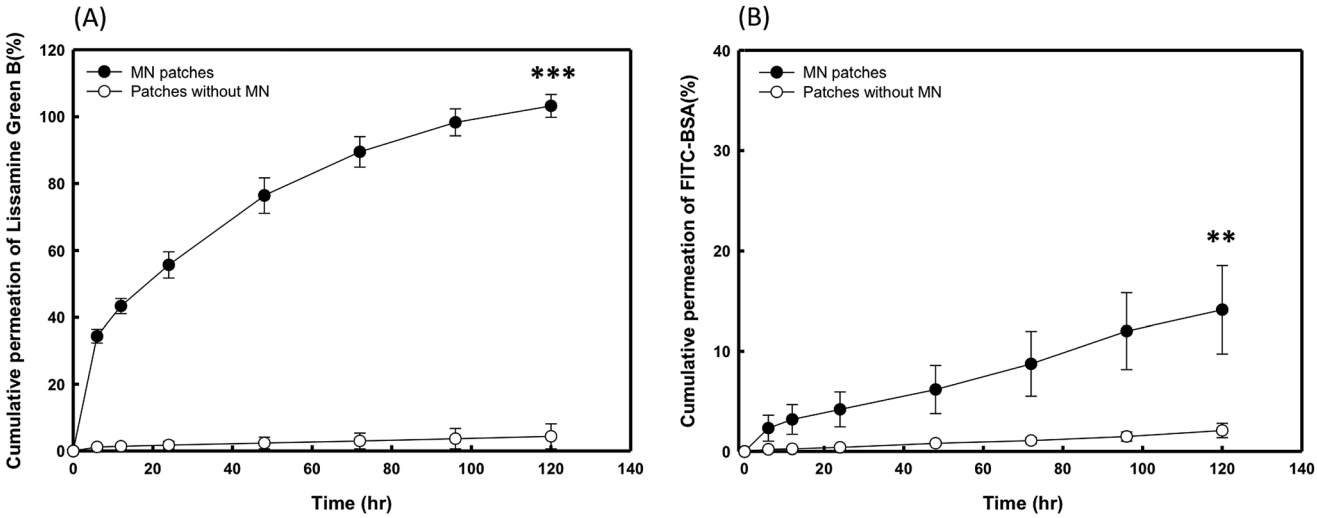

Fig. 6 *In vitro* transdermal drug-release profiles of LGB- and BSA-FITC-loaded PVP MNs into porcine ear skin *via* the PVP360/PVP10 1 : 3 MN patches. (A) Cumulative permeation of LGB. (B) Cumulative permeation of BSA-FITC.

difficult to apply on the skin. To improve the flexibility of the backing layer of MN patches, 25% CMC was added to the 30% PVP360 solution to form a backing layer, as in process B in Fig. 1. Fig. 7(A, a and b) show the morphologies of PVP-based MNs with a backing layer composed of 30% PVP360 and 30% CMC/PVP360 = 3 : 1, respectively. The backing layer composed of CMC/PVP360 is more flexible and suitable for animal studies than PVP360 alone. The blood glucose levels of diabetic mice after application are shown in Fig. 7(B). It is revealed that the maximum decrease in glucose levels appeared 2 hours after application in both the PVP-based MN patch group and the SC injection with insulin group. In addition, the blood glucose levels of insulin-loaded PVP-based MN patches and subcutaneous group after 2 hours of application were approximately 13.57 ± 2.27% and 16.63 ± 3.48% of initial levels, respectively. The results demonstrated that the PVP MN patch displays an efficient release and delivery effect. In addition, the PVP MN patch has a similar effect to hypodermic injection on hypoglycemic administration. Furthermore, the analysis of the pharmacodynamic parameters of glucose level is also shown in Fig. 7(C). The total area above the glucose level *versus* time curve as an index of hypoglycemic effect was 288.49 ± 8.23% h at 0.2 IU kg^{-1}. The RPA of insulin from the PVP-based MN patch were 108.74%. The *in vivo* study shows that the PVP-based MNs

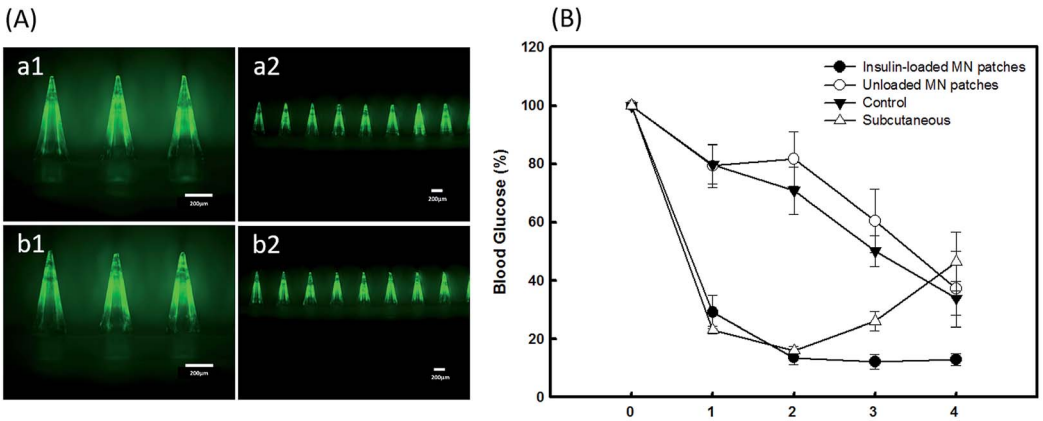

(C)

Group	*C*min (%)	*T*min (h)	AAC (%h)	RPA (%)
Unloaded MN patches	37.15±13.06	4	132.36±12.55	-
Insulin-loaded MN patches (0.2IU)	13.57±2.27	2	288.49±8.23	108.74
Subcutaneous (0.2IU)	16.63±3.48	2	265.3±8.88	100

Fig. 7 *In vivo* drug release profiles of insulin-loaded PVP360/PVP10 MNs and hypodermic injection in diabetic mice. (A) Morphologies of insulin-FITC MN patches with backing layers composed of 30% PVP360 (a1–a2) and 30% PVP360/CMC 3 : 1 (b1–b2). (B) Blood glucose level *versus* time. (C) Pharmacodynamic parameters of insulin after administration of dissolving MN patches in diabetic mice.

dissolved into the skin immediately after application, and insulin is released from the MN patch and delivered into the circulatory system. This results in an efficient regulation of glucose levels. In addition, Fig. 7(B) shows that glucose levels continue to be maintained at a low level 4 hours after application in the PVP MNs group, which is lower than the hypodermic injection group. Kaneda *et al.* have used PVP as a polymeric carrier and found that PVP showed the longest mean retention time after IV injection of all nonionic polymers with the same molecular size, which revealed that PVP may be used to improve the plasma half-live of the drug.[24] Additionally, they illustrated that PVP had the longest circulation time, and its tissue distribution was significantly restricted. Therefore, it is suggested that PVP may bind to plasma proteins and affect the pharmacodynamic parameters of glucose levels, resulting in more long-term regulation compared with insulin injections. Thus, MNs composed of PVP may extend the half-life of the drug and help glycemic control.

In this study, the PVP-based MNs demonstrated good penetration ability and achieved efficient TDD of the model drug, which provided an alternative for treating diabetes. The two-layer PVP-based MNs prepared using a gentle and organic solvent-free technique that avoids harsh fabrication environments may be used for protein drug encapsulation. The two-layer PVP-based MNs prepared using a gentle and organic solvent-free technique that avoids harsh fabrication environments may be used for protein drug encapsulation. In addition, this transdermal delivery system may also provide the possibility to encapsulate several acesodyne and anticancer drugs such as lidocaine, sumatriptan, or aminolevulinic acid. Moreover, skin represents a good target for delivery of vaccine as an alternative to the conventional intramuscular route of immunization. The fabrication procedure of PVP-based MNs is appropriate for protein loading which may also provide a feasible application for MN vaccination.

4 Conclusions

A dissolving PVP-based MN patch with two molecular weights of PVP was successfully fabricated. This transdermal delivery system provides the advantages of drug localization and efficiency enhancement, patient-friendly use, and painlessness. The needle tips prepared using PVP360/PVP10 provide better penetration ability but do not influence the solubility and backing layer prepared using CMC/PVP360 to improve the flexibility for skin fitting. The PVP-based MN patch provides immediate and efficient delivery for self-administration and may become an alternative tool for pharmaceutical transportation.

Acknowledgements

We acknowledge financial support from Chang Gung University. This work was supported by grants from the Chang Gung Memorial Hospital (Summit Project Grants: CMRPD1C0421-22 and CMRPD1C0431-32). The authors especially acknowledge technical support by Jwu-Ching Shu for the induction of diabetic mice and instrumentation support (OCT microscopy) by Meng-Tsan Tsai.

References

1 I. Singh and A. P. Morris, *Int. J. Pharm. Invest.*, 2011, **1**, 4–9.
2 M. R. Prausnitz and R. Langer, *Nat. Biotechnol.*, 2008, **26**, 1261–1268.
3 M. R. Prausnitz, *Adv. Drug Delivery Rev.*, 2004, **56**, 581–587.
4 M. Hultstrtröm, N. Roxhed and L. Nordquist, *J. Diabetes Sci. Technol.*, 2014, **8**, 453–457.
5 M. C. Chen, K. Sonaje, K. J. Chen and H. W. Sung, *Biomaterials*, 2011, **32**, 9826–9838.
6 D. R. Owens, B. Zinman and G. Bolli, *Diabetic Med.*, 2003, **20**, 886–898.
7 M. H. Ling and M. C. Chen, *Acta Biomater.*, 2013, **9**, 8952–8961.
8 I. C. Lee, W. M. Lin, J. C. Shu, S. W. Tsai, C. H. Chen and M. T. Tsai, *J. Biomed. Mater. Res., Part A*, 2017, **105**, 84–93.
9 K. Matsuo, Y. Yokota, Y. Zhai, Y. S. Quan, F. Kamiyama, Y. Mukai, N. Okada and S. Nakagawa, *J. Controlled Release*, 2012, **161**, 10–17.
10 Z. Zhu, H. Luo, W. Lu, H. Luan, Y. Wu, J. Luo, Y. Wang, J. Pi, C. Y. Lim and H. Wang, *Pharm. Res.*, 2014, **31**, 3348–3360.
11 M. J. Garland, E. Caffarel-Salvador, K. Migalska, A. D. Woolfson and R. F. Donnelly, *J. Controlled Release*, 2012, **159**, 52–59.
12 K. Migalska, D. I. Morrow, M. J. Garland, R. Thakur, A. D. Woolfson and R. F. Donnelly, *Pharm. Res.*, 2011, **28**, 1919–1930.
13 J. W. Lee, J. H. Park and M. R. Prausnitz, *Biomaterials*, 2008, **29**, 2113–2124.
14 W. Chen, C. Wang, L. Yan, L. Huang, X. Zhu, B. Chen, H. J. Sant, X. Niu, G. Zhu, K. N. Yu, V. A. L. Roy, B. K. Gale and X. Chen, *J. Mater. Chem. B*, 2014, **2**, 1699–1705.
15 S. P. Sullivan, N. Murthy and M. R. Prausnitz, *Adv. Mater.*, 2008, **20**, 933–938.
16 Y. K. Demir, Z. Akan and O. Kerimoglu, *PLoS One*, 2013, **8**, e63819.
17 K. Tsioris, W. K. Raja, E. M. Pritchard, B. Panilaitis, D. L. Kaplan and F. G. Omenetto, *Adv. Funct. Mater.*, 2012, **22**, 330–335.
18 S. A. Papadimitriou, P. Barmpalexis, E. Karavas and D. N. Bikiaris, *Eur. J. Pharm. Biopharm.*, 2012, **82**, 175–186.
19 S. O. Rogero, S. M. Malmonge, A. B. Lugao, T. I. Ikeda, L. Miyamaru and Á. S. Cruz, *Artif. Organs*, 2003, **27**, 424–427.
20 I. C. Lee, J. S. He, M. T. Tsai and K. C. Lin, *J. Mater. Chem. B*, 2015, **3**, 276–285.
21 Y. Ito, M. Hirono, K. Fukushima, N. Sugioka and K. Takada, *Int. J. Pharm.*, 2012, **436**, 387–393.
22 Y. Ito, S. Kashiwara, K. Fukushima and K. Takada, *Drug Dev. Ind. Pharm.*, 2011, **37**, 1387–1393.
23 K. Fukushima, A. Ise, H. Morita, R. Hasegawa, Y. Ito, N. Sugioka and K. Takada, *Pharm. Res.*, 2011, **28**, 7–21.
24 Y. Kaneda, Y. Tsutsumi, Y. Yoshioka, H. Kamada, Y. Yamamoto, H. Kodaira, S. Tsunoda, T. Okamoto, Y. Mukai, H. Shibata, S. Nakagawa and T. Mayumi, *Biomaterials*, 2004, **25**, 3259–3266.